HAL
open science

Clinical and preclinical imaging of hepatosplenic schistosomiasis.

Brice Masi, Teodora-Adriana Perles-Barbacaru, Monique Bernard, Angèle Viola

To cite this version:

Brice Masi, Teodora-Adriana Perles-Barbacaru, Monique Bernard, Angèle Viola. Clinical and preclinical imaging of hepatosplenic schistosomiasis.. Trends in Parasitology, 2020, 36 (2), pp.206-226. 10.1016/j.pt.2019.11.007 . hal-02412606

HAL Id: hal-02412606

https://amu.hal.science/hal-02412606v1

Submitted on 14 Sep 2020

HAL is a multi-disciplinary open access archive for the deposit and dissemination of scientific research documents, whether they are published or not. The documents may come from teaching and research institutions in France or abroad, or from public or private research centers.

L'archive ouverte pluridisciplinaire **HAL**, est destinée au dépôt et à la diffusion de documents scientifiques de niveau recherche, publiés ou non, émanant des établissements d'enseignement et de recherche français ou étrangers, des laboratoires publics ou privés.

Clinical and preclinical imaging of hepatosplenic schistosomiasis

Brice Masi, Teodora-Adriana Perles-Barbacaru*, Monique Bernard and Angèle Viola*

CNRS, Aix-Marseille Université, CRMBM, Faculté des Sciences Médicales et Paramédicales la Timone, 27 boulevard Jean Moulin, Marseille, FRANCE.

*Correspondence: angele.viola@univ-amu.fr (A. Viola) and teodora.perles-barbacaru@univ-amu.fr (T. Perles-Barbacaru)

Keywords: hepatosplenic schistosomiasis, liver fibrosis, portal hypertension, clinical imaging, preclinical imaging, quantitative imaging methods

Abstract

Schistosomiasis, a neglected tropical disease, is a major cause of chronic morbidity and disability, and premature death. The hepatosplenic form of schistosomiasis is characterized by hepatosplenomegaly, liver fibrosis, portal hypertension and oesophageal varices, whose rupture may cause bleeding and death. We review currently available abdominal imaging modalities and describe their basic principles, strengths, weaknesses, and usefulness in the assessment of hepatosplenic schistosomiasis. Advanced imaging methods are presented that could be of interest for hepatosplenic schistosomiasis evaluation by yielding morphological, functional and molecular parameters of disease progression. We also provide a comprehensive view of preclinical imaging studies and current research objectives such as parasite visualisation in hosts, follow-up of host-immune response, and development of non-invasive quantitative methods for liver fibrosis assessment.

26 **Hepatosplenic schistosomiasis**

27 Schistosomiasis, a waterborne helminthic disease is a major cause of chronic morbidity and
28 premature death in Africa, South America, South East Asia, and Middle East, whereas imported
29 cases have recently been on the rise in Europe. *Schistosoma mansoni* and *Schistosoma*
30 *japonicum* are the main causative agents of hepatosplenic schistosomiasis (HSS). Schistosome
31 eggs eliminated with mammalian excreta hatch in water and release miracidia that infect
32 specific intermediate host snails. The gastropods shed on cercariae that can penetrate the skin
33 of the human host. These larvae transform into schistosomulae, migrate to the venous
34 circulation, and differentiate into sexually mature worms [1, 2]. The eggs laid in the mesenteric
35 vessels (*S. mansoni, S. japonicum*) migrate to the gastrointestinal tract and the liver. The host
36 immune response leads to egg encapsulation within layers of immune cells embedded in
37 extracellular matrix (ECM). Granuloma formation is a cause of chronic inflammation and
38 fibrosis (Box 1) [1]. The diseases caused by *S. mansoni* and *S. japonicum* are divided in two
39 stages, the acute and chronic phases. The acute syndrome generally occurs in the first infection,
40 in the first months after exposure. In the chronic phase, two main clinical forms of
41 schistosomiasis may occur, the hepatointestinal or the hepatosplenic disease [3].

42 The hepatosplenic complication occurs in less than 10% of patients, 5–20 years after infection
43 [4, 5], owing to chronic granulomatous inflammation in the liver, leading to severe fibrosis of
44 the portal system (Figure 1, Key Figure). Hepatomegaly is often an early sign of granulomatous
45 inflammation [1, 6]. Fibrosis in HSS occurs with little hepatocellular damage unlike cirrhosis
46 (Box 1) [5, 7]. The major complication of liver fibrosis is portal hypertension (PH) (Box 1),
47 which causes splenomegaly and esophageal, gastric, splenorenal, pancreaticoduodenal and
48 periumbilical varice formation. Esophageal varice bleeding is potentially fatal [1, 2, 5, 8]. Other
49 complications include anemia, thrombocytopenia, nephritic glomerulopathy, and pulmonary
50 arterial hypertension with right heart failure [1, 2, 5, 8]. Liver dysfunction may occur in cases

of comorbidities (hepatitis, steatosis) (Box 1) [5] and in advanced-stage disease. HSS is associated with a higher incidence of hepatocellular carcinoma [2]. The diagnosis of parasite infection is generally based on fecal egg count (Kato-Katz technique) and requires sexually mature worms. Rectal mucosa biopsy for egg detection is performed when infection is suspected despite negative Kato-Katz tests. The diagnosis of HSS relies on clinical examination, liver biopsy and medical imaging. Changes in size and consistency of the liver and the spleen can be detected at palpation and percussion. Biopsy, the standard diagnostic technique is highly invasive and tissue sampling often inadequate to cover fibrosis heterogeneity. **Ultrasonography** (USG, see Glossary) is currently the most widely used technique to detect organomegaly and altered texture due to fibrosis [9, 10].

Overview of imaging modalities and applications to HSS

Imaging allows the assessment of HSS morbidity by diagnosing and staging fibrosis, evaluating vascular complications, guiding surgical interventions, and monitoring response to treatment. Improving fibrosis diagnosis and staging, especially early and mild forms, with non-invasive and quantitative methods is a major challenge in liver imaging, regardless of the cause of fibrosis. Preclinical imaging studies are essential to better characterize specific morphologic and functional changes linked to granulomatous inflammation. They are also required for the development and validation of imaging methods with improved sensitivity to early fibrosis, and for the identification of robust biomarkers translatable to the clinical setting.

This review provides an update on HSS imaging, covering clinical and research applications. After a methodological overview of abdominal imaging modalities, we discuss their utility in the diagnosis and follow-up of HSS. We describe multimodal approaches combining imaging techniques with **elastography** and the results obtained so far on HSS. We discuss the potential of advanced methods evaluated in the research setting that could take up the challenge of non-

76 invasive quantitative assessment of fibrosis severity and vascular dysfunction. We also provide
77 the first synthesis of preclinical imaging studies and present the main lines of research including
78 parasite visualization in hosts, follow-up of host-immune response, and development of non-
79 invasive quantitative methods for HSS assessment.

80 ***Ultrasonography (USG)***

81 USG is the first-line medical imaging examination for the non-invasive exploration of
82 gastrointestinal and hepatic diseases (Table 1). Real-time imaging of parenchymal texture,
83 vascular anatomy and haemodynamics allows fast clinical interpretation as well as guidance of
84 interventional procedures and monitoring response to therapy.

85 Due to its portability and cost-effectiveness, USG is also the most-widely used radiologic
86 method to diagnose HSS (Table 2). Although HSS caused by *S. mansoni and S. japonicum*
87 share common features, differences in fibrotic lesions have been described such as the
88 "mosaics" formed by echogenic septa [11-14] in *S. japonicum* infection. The need for fibrosis
89 scales specific for HSS and standardized USG methods for schistosomiasis exploration led to
90 consensus guidelines. The landmark Niamey classification specific for the mansonian disease
91 includes scores for liver parenchymal patterns, periportal fibrosis and PH [15]. Granulomatous
92 inflammation is described as pattern B or "starry sky" (Figure 1) because of diffuse echogenic
93 spots. Fibrosis along portal sub-branches is described in pattern C as "rings" and "pipestems"
94 depending on the viewing angle, and as "bull's eye" on cross-sections with an anechogenic
95 portal vein surrounded by echogenic fibrous tissue. Fibrosis can also be localized around the
96 portal vein bifurcation as "ruff" (pattern D). USG permits to measure fibrosis thickness of
97 second order branches, of the gallbladder as well as ruff thickness. In advanced forms, patches
98 form around the hepatic portal vessels for pattern E and extend to the liver periphery as "Bird's
99 claw" for pattern F. Combinations of patterns are possible (e.g. iDb, Dc, Ec). PH is evaluated
100 by measuring portal vein diameter, second order branch dilation, splenic vein diameter and by

101 detecting varices. Volumetric assessment of the liver is possible with newer USG systems.
102 Spleen enlargement and texture (homogenous or granular) can be evaluated. Ascites, masses
103 such as cancers (pattern Z) or haemangioma can be detected. The differential diagnosis between
104 cirrhosis and schistosomiasis is complicated by the presence of intraparenchymal fat (*e.g.*
105 alcoholic and non-alcoholic steatosis) resulting in hyperechogenicity of the parenchyma. In this
106 case, pattern Y is assigned. Systemic varices and portal vein thrombosis can be detected by
107 analysing blood flow using Doppler ultrasound.
108
109 ***Computed tomography (CT)***
110 **CT** is widely used to explore diffuse or focal digestive diseases (Table 1). There are few CT
111 studies on liver fibrosis [16]. Analysis of texture features from CT images enables staging of
112 fibrosis throughout the liver, but is less accurate in case of heterogeneous fibrosis and
113 considered inferior to ultrasound transient elastography (TE, FibroScan®) [17]. PH can be
114 diagnosed by portal vein and mesenteric vein dilation, varices and organomegaly detectable
115 with a single rapid scan. Repeated scanning during injection of mainly tri-iodinated benzene
116 ring-containing contrast agents (**CA**) allows identification of arterial, venous and perfusion
117 phases with the potential to detect perfusion changes occurring during fibrosis, but delivers
118 higher radiation dose. Increased parenchymal CA retention is observed in advanced fibrotic
119 tissue.
120 Unexpected hepatic and pancreatic lesions have been described in the acute phase of *S. mansoni*
121 infection together with hepatomegaly and splenomegaly [18] (Table 2). In mansonian HSS, the
122 main features of the fibrotic liver are round low-density periportal zones enhancing after CA
123 administration, and linear bands in longitudinal sections of portal veins [19]. In HSS caused by
124 *S. japonicum,* capsular and septal calcifications result in a "turtle back" appearance of the liver.
125 Fibrous septa are enhanced after CA injection [11-13, 20-22].

126

127 ***Magnetic resonance imaging (MRI)***

128 Anatomy, microstructure, vasculature, perfusion, and metabolism can be assessed with
129 magnetic resonance methods (Table 1). In the portal venous phase and the delayed venous
130 phase, unspecific extracellular gadolinium chelates enhance fibrous hepatic tissue, and improve
131 texture analysis [23]. Clinically approved hepatocyte-specific CAs such as Gadoxetate
132 Disodium (Gd-EOB-DTPA) employed for diagnosing and staging HCC are used to assess the
133 residual liver tissue function in liver fibrosis [24].

134 MRI would provide more precise information than USG regarding periportal fibrosis,
135 gallbladder fibrosis, and alterations of the abdominal venous system in HSS (Table 2) [4, 25].
136 Besides the detection of morphological anomalies suggestive of liver fibrosis and PH on
137 anatomical images (splenomegaly, large portal vein diameter, varices, ascites…) [4, 14],
138 granulomatous inflammation and liver fibrosis can be detected on CA-enhanced MRI, and
139 various methods can be used to assess subtle changes in liver microstructure [26]
140 (Supplementary file).

141

142 ***Scintigraphy, single-photon emission computed tomography (SPECT), positron emission***
143 ***tomography (PET)***

144 Although the main applications of nuclear medicine techniques are in oncology (Table 1),
145 scintigraphy can be used to stage PH and portosystemic shunts in chronic liver diseases [27],
146 whereas ^{18}F-fluorocholine radiotracer seems promising for the grading of liver fibrosis [28].
147 Differentiation between cirrhotic and non-cirrhotic PH is possible with ^{99m}Tc-labelled sulphur
148 colloid particles but specific fibrosis patterns pathognomonic for schistosomiasis are not
149 discernible. Scintigraphy has been used in the post-operative follow-up of patients who
150 underwent splenectomy followed by auto-implantation of spleen tissue [29, 30]. A case report

151 described hypermetabolic pancreatic lesions with **deoxy-2-(^{18}F)fluoro-D-glucose** in HSS [31].
152 Interestingly, hepatic angioscintigraphy with ^{99m}Tc-labelled sulphur colloid particles revealed
153 increased hepatic perfusion index in patients with HSS, which was correlated with
154 splenomegaly and oesophageal varices [32]. This finding would reflect an increased perfusion
155 through the hepatic artery (Table 2).
156
157 ***Endoscopy and laparoscopy***
158 **Endoscopy** can be used for diagnosis, biopsy, follow-up, and therapeutic purposes (*e.g.*
159 laparoscopic surgery, image-guided embolization or ligation of varices) (Table 1).
160 HSS can be explored by endoscopy (Table 2) [33]. The cost and risk of infection linked to the
161 invasiveness of the technique are limitations to its use in resource-limited countries. Endoscopy
162 permits to view and treat collaterals, to identify ascites, PH, whereas hepatomegaly,
163 splenomegaly and granulomatous inflammation in liver can be detected with laparoscopy.
164 Endoscopy is the gold-standard technique to guide ligation or sclerotherapy treatment of
165 oesophageal varices. In HSS with PH, endoscopic sclerotherapy for esophageal varices was
166 shown to be more efficient for secondary prophylaxis of upper gastrointestinal bleeding when
167 preceded by splenectomy and esophagogastric devascularisation [34].
168
169 **Which imaging modality for which HSS stage?**
170 The acute stage is characterized by a syndrome with severe clinical manifestations including
171 hepatomegaly, splenomegaly and lymphadenopathy. The enlargement of the liver, the spleen
172 and abdominal lymph nodes can be visualized with USG [35]. When other sites of lesions are
173 suspected during this stage (e.g. central nervous system, lungs or intestines…), other imaging
174 modalities more appropriate for the exploration of these organs should be utilized (CT, MRI or
175 endoscopy). Regarding the chronic phase, physical examination and laboratory findings may

176 not always permit to classify patients, especially if the time of infection is unknown. Moreover,
177 there are frequent overlaps of the pathological signs of the acute and chronic stages, and of
178 moderate and severe HSS (Table 2). Fibrosis and PH are common features of both moderate
179 and severe HSS, but PH predominates in severe HSS and is associated with congestive
180 splenomegaly and a high risk of variceal bleeding. Fibrosis grade is regarded as a predictive
181 value for PH and esophageal varices. USG, the first line imaging modality, permits the detection
182 of splenomegaly, fibrosis, and hemodynamic changes. Although USG can be used for fibrosis
183 grading, it is not sensitive to mild disease, and often underestimates fibrosis in comparison to
184 liver biopsy [14], and is sensitive to inflammation [35]. If available, conventional CT or MRI
185 methods can be used to map fibrosis spatial distribution [5, 36]. As for USG, the results may
186 be affected by inflammation in early disease stages. Fibrogenesis and inflammation are
187 generally concomitant processes and such indirect parameters are not sufficiently specific.
188 (Supplementary file). Additional investigation can be performed with SWI to detect iron
189 deposits in inflammatory processes. When using CT or MRI, additional hemodynamic
190 parameters can be collected with DCE or ASL. All these methods are available on clinical MRI
191 scanners.
192
193
194
195 **Emerging methods for human schistosomiasis assessment?**
196
197 ***Evaluation of liver fibrosis***
198 *Elastography* - Elastography has become the most widely used method to detect liver fibrosis
199 and cirrhosis consecutive to steatosis or viral hepatitis [37]. Elastography cannot be regarded
200 as an emerging method, but so far only few studies have reported its use in HSS.

201 In sonographic elastography, tissue excitation is either induced by acoustic radiation force
202 impulse (ARFI) or using a mechanical vibrating device for TE. Pulse-echo acquisitions are
203 performed to measure the velocity of the shear-wave, which informs about the elastic properties
204 of the tissue. Few studies have explored HSS using sonographic elastography (Table 3) and
205 only one used the ARFI method (Table 3). In patients with hepatitis C virus co-infection
206 discrepancies between liver biopsy and ultrasonographic TE findings were identified [38, 39],
207 probably due to fibrosis heterogeneity. In the absence of comorbidities, liver stiffness
208 measurement (LSM) was higher in HSS patients than in controls and cirrhotic patients [40, 41].
209 One single study evaluating both liver and spleen stiffness reported a correlation between
210 spleen stiffness and some USG signs of PH (portal vein diameter, area, and congestion index,
211 splenic artery resistance index, splenic vein diameter and spleen diameter) [41]. In *S. japonicum*
212 HSS, LSM was not correlated to USG findings [42]. These studies suggest that liver LSM could
213 be a marker of HSS fibrosis. Moreover, spleen stiffness could assist in selecting patients for
214 endoscopy. Indeed, it would be superior to liver stiffness in predicting esophageal varices [43].
215 However, ultrasound TE has several limitations, including a lack of reproducibility/reliability
216 in case of steatosis, light fibrosis, obesity or ascites. Moreover, liver stiffness is affected by
217 inflammation, iron overload, blood flow, and venous congestion [37, 44, 45].
218 Mechanically generated shear waves propagating through the liver can also be detected using
219 motion-sensitive MRI techniques [37] implemented on standard MRI systems. Magnetic
220 resonance elastography (MRE)-derived stiffness correlates with fibrosis stage in patients [46].
221 MRE appears more accurate and reliable than USG elastography to stage fibrosis [45, 47-50]
222 and allows better coverage of fibrosis heterogeneity [37], moreover it is reliable in case of
223 ascites. However, confounding comorbidities such as iron overload can limit the reliability of
224 MRE.

225 *Advanced MRI methods* - MRI methods sensitive to Brownian water motion in tissues are used
226 to probe tissue microstructure. Diffusion-weighted imaging (based on Gaussian distribution of
227 water diffusion) with apparent diffusion coefficient (ADC) mapping, diffusion kurtosis imaging
228 (based on non-gaussian distribution of water diffusion) have been successfully applied to stage
229 moderate to advanced fibrosis in pre-cirrhotic liver with equal performance [51, 52]. Intravoxel
230 incoherent motion (IVIM) analysis which separately assesses parenchymal diffusion and
231 microvascular perfusion changes could be potentially more sensitive to pathophysiological
232 alterations during early fibrosis [53].
233 Double contrast-enhanced MRI using gadolinium-based CAs and SPIOs with or without texture
234 analysis has been used to differentiate early liver fibrosis from advanced disease with excellent
235 results [23, 54, 55]. Collagen fiber deposition in the space of Disse leads to an increase of the
236 extracellular space quantifiable as the distribution volume fraction of nonspecific CA in the
237 parenchymal (equilibrium) phase by MRI (or CT) [56-59]. Preclinical studies have shown that
238 the liver accumulation of collagen targeted CAs correlates with histological fibrosis scores [60].
239 Non-contrast enhanced relaxometric studies quantifying the longitudinal (T_1), transverse (T_2*)
240 and combined ($T_1\varrho$) magnetic relaxation time constants, which provide information on tissue
241 microstructure and macromolecule content, have shown a good correlation of these parameters
242 with liver fibrosis, without being specific for it [61-64]. (Supplementary file).
243 *Phosphorus magnetic resonance spectroscopy (^{31}P-MRS)* - **MRS** is a non-invasive method for
244 monitoring cellular metabolism that can be performed during an MRI exploration. Spectra are
245 often acquired from a unique **voxel** (single voxel spectroscopy, SVS). MRS imaging (MRSI)
246 permits the simultaneous acquisition of multiple spectra in contiguous voxels and the
247 generation of metabolic maps providing spatial distribution of metabolite signals. ^{31}P-MRS
248 allows assessment of bioenergetics and phospholipid metabolism intermediates mainly
249 phosphomonoesters (PME) and phosphodiesters (PDE) (Box 1). An alteration of phospholipid

250 metabolism in cirrhosis has been identified using SVS and MRSI techniques [65, 66]. Fibrosis
251 was associated with a decrease in PDE and the PME/(PME+PDE) ratio could separate mild
252 from advanced fibrosis [65]. In another study, the PME/PDE ratio was strongly correlated with
253 advanced fibrosis [66]. (Supplementary file).
254
255 ***Assessment of vascular damage***
256 *Detection of varices with non-invasive capsule endoscopy* - Capsule endoscopy involving
257 transit of an ingestible wireless camera along the digestive tract can be performed to visualise
258 the entire small bowel when simultaneous therapeutic intervention or tissue sampling is not
259 required. Capsule endoscopy has been successfully used in a pilot study to detect oesophageal
260 varices in HSS and enabled the identification of small bowel lesions in PH together with edema,
261 erosions and scarred mucosa [67, 68]. Although clinically significant esophageal and rectal
262 varices are typically visible endoscopically, ectopic varices may require cross sectional or
263 multiplanar portal venous phase CT or MRI for diagnosis.
264 *Assessment of liver perfusion* - Besides the non-invasive delineation of hepatic vascular
265 anatomy by CT and MRI angio- and portography, several methods can be used for the
266 assessment of hemodynamic changes in liver pathologies, including cirrhotic or non-cirrhotic
267 PH. Among them, **dynamic contrast-enhanced** (DCE) CT, MRI or USG, relying on CA
268 injection and liver-specific tracer kinetic modelling, allows quantitative assessment of liver
269 perfusion and separation of arterial and portal-venous phases [69, 70]. DCE MRI studies
270 showed that reduced portal perfusion was quantitatively related to fibrosis stage [71].
271 Hemodynamic parameters obtained from DCE imaging, such as increased mean transit time
272 [72] and arterial blood flow [73], have the potential to detect perfusion changes occurring early
273 during fibrosis. Non-invasive and quantitative tissue perfusion measurement can also be
274 performed **with arterial spin labelling** (ASL) techniques without exogenous CA. These

275 techniques developed for the heart, kidney and brain have been successfully applied to the liver.
276 A significant reduction in liver and spleen perfusion could be measured in cirrhosis [74, 75].
277 Although ASL has not yet been implemented in the clinical abdominal MRI routine, it
278 represents an alternative to standard DCE methods, when repeated measures are required or
279 when CA injection is contraindicated.
280 Quantitative MRI providing blood velocity in all directions and over the entire cardiac cycle,
281 now feasible within tenth of minutes, can depict altered flow patterns in the abdominal
282 vasculature, revealing PH and its consequences such as portocaval anastomoses less accessible
283 by USG, Doppler US or endoscopy.
284 *MRI detection of splenic siderotic nodules* - **Diffusion MRI** with ADC mapping of the spleen
285 [41] and magnetic susceptibility-weighted imaging (SWI) [76, 77] have been successfully used
286 to evaluate splenic signs of PH including splenic siderotic nodules (Gamna-Gandy bodies) (Box
287 1) with higher sensitivity than anatomical MRI. Although these nodules are a frequent sign (>
288 65%) of PH in HSS [78, 79], SWI which is sensitive to iron deposits, has not yet been applied
289 in HSS. SWI as well as quantitative susceptibility mapping (QSM) is also sensitive to
290 calcifications, which are frequent in *S. japonicum* infection, and to hemorrhages. SWI has
291 shown high accuracy for the grading of mild and advanced liver fibrosis [77, 80].
292
293 **Pre-clinical imaging studies of schistosomiasis**
294 ***Animal models***
295 Models of schistosomiasis have been developed in different animal species providing the
296 opportunity to study host immune response to schistosome infection, granulomatous
297 inflammation, fibrogenesis, and to evaluate new therapies or vaccine candidates. Although they
298 do not recapitulate all the features of the human disease, they remain clinically relevant as they
299 develop liver fibrosis [81] and PH [82]. The characterization of experimental HSS with imaging

300 methods is essential for the selection of appropriate models in pharmacological studies.
301 Preclinical studies aim at developing methods allowing direct visualisation and quantification
302 of the parasites within host tissues, monitoring of host immune response to schistosome,
303 detection, staging and quantification of liver fibrosis, and identification of markers for assessing
304 anti-parasitic or anti-fibrotic drug efficacy (Table 4).
305
306 ***Imaging parasites within host tissues***
307 *In vivo* visualisation of schistosomes at different developmental stages could help monitor
308 parasite burden, detect ectopic localization and assess the schistosomicidal efficacy of new
309 chemotherapies. Using **fluorescence molecular tomography** (FMT) [83] and microPET in
310 mice, adult worms of different species (S. *mansoni, S. japonicum* and *S. haematobium* the agent
311 of urogenital schistosomiasis) were directly visualized [84] and the anti-helminthic efficacy of
312 several drugs could be monitored. FMT was used alone or in combination with microPET and
313 MRI [85]. MicroPET studies showed that (^{18}F)FDG was taken up by *S. mansoni* worms in mice
314 (Table 4).
315 Confocal laser scanning microscopy combined with a lens system integrated in a rigid
316 endoscope was tested for the visualisation of eggs within the gut mucosa of mice infected with
317 *S. mansoni* [86]. Detection and differentiation between viable and dead eggs was achieved in
318 real time during endoscopy. Although performed on euthanized animals, this technique is a
319 potential substitute for invasive tissue sampling when stool specimens are negative in early
320 infection or due to treatment. The technique was applied shortly after to detect eggs in the
321 bladder mucosa of a *S. haematobium* infected patient [87]. Fluorescent CA targeting eggs could
322 possibly increase sensitivity of the endoscopic approach.
323 ***Monitoring host immune response***

324 **Bioluminescence imaging** (BLI), a method allowing direct visualisation of gene expression
325 through chemically-induced light emission [88, 89] was used to follow up eosinophilia and
326 eosinopoiesis in mice infected with *S. mansoni* and expressing a luciferase reporter driven by
327 an eosinophil peroxidase promoter [90]. In another study, the dynamics of collagen deposition
328 in *S. japonicum* infection were monitored in mice expressing luciferase under a collagen
329 promotor [91]. Newly formed collagen was assessed in mice with and without praziquantel
330 treatment after granuloma formation.

331 ***Characterization of HSS and identification of imaging markers of fibrosis***

332 HSS has been investigated with SPECT/CT, MRI, and USG (Table 4). USG studies in *S.*
333 *japonicum* infected mice, rabbits and pigs identified common features with the human disease
334 including hepatomegaly, advanced liver fibrosis, and enlarged portal vein diameter. A
335 longitudinal study of the mouse model provided further description of HSS including portal and
336 splenic vein diameter, spleen and liver morphometry, liver fibrosis patterns, and intestinal wall
337 thickening [92]. These studies confirmed the relevance of experimental models of *S. japonicum*
338 infection in pathophysiological and pharmacological studies.

339 HSS in *S. mansoni* infection was investigated in experimental models (mice) and semi-captive
340 chimpanzees. As for *S. japonicum* infection, the imaging studies demonstrated the relevance of
341 these models to the characterization of HSS. A longitudinal study performed on *S. mansoni*
342 infected mice using microSPECT/CT and a new radiotracer labeled with ^{188}Re (^{188}Re-OCTAM)
343 binding to hepatocyte asialoglycoprotein receptors (Box 1) permitted to detect hepatic necrosis
344 and fibrosis [93]. The first MRI study of *S. mansoni* infected mice [94] used anatomical MRI
345 and identified a patchy liver pattern assigned to fibrosis at histology. A longitudinal MRI study
346 of this model [95] revealed anatomical signs of PH (liver, spleen and portal vein enlargement)
347 and contrast-enhancement of fibrotic liver lesions. Furthermore, this study proposed that

quantitative mapping of the transverse T_2 relaxation time constant could be used to non-invasively assess fibrosis [95].

Concluding remarks

Assessment of HSS morbidity and treatment monitoring would benefit from non-invasive imaging methods allowing reliable fibrosis staging and estimation of vascular dysfunction (see outstanding questions). Quantitative methods, which have been successfully evaluated on human fibrotic and cirrhotic liver (USG elastography, MRE, ^{31}P-MRS, ASL, perfusion PET …) or in experimental schistosomiasis (T_2 mapping) have a potential for clinical/human schistosomiasis assessment provided the equipment is available. Advanced acquisition and post-processing methods under development aiming at identifying markers sensitive to early pathological mechanisms (inflammation, perfusion changes) and early fibrosis stages (*e.g.* IVIM, combined arterial and portal venous input DCE, double-contrast enhanced MRI) still require validation in schistosomiasis models. Moreover, the precise relationship between imaging markers (*e.g.* relaxation time constants or ADC) and pathophysiological changes accompanying chronic hepatic inflammation (iron accumulation and edema) as well as the possible contributions of confounding factors such as comorbidities (steatosis, hepatitis) need to be established. Non-invasive markers of hepatic fibrosis are increasingly needed in pharmacological studies prompting the development of advanced and standardized quantitative methods with translational potential in clinics.

Funding: this work was funded by CNRS (Centre National pour la Recherche Scientifique) and Aix-Marseille University. CRMBM is a member of France Life Imaging (grant ANR-11-INBS-0006 from the French “Investissements d’Avenir” program).

373 **Declarations of interest:** none

374

375 **References**

376 1. Ross, A.G. et al. (2002) Schistosomiasis. N Engl J Med 346 (16), 1212-20.

377 2. Colley, D.G. et al. (2014) Human schistosomiasis. Lancet 383 (9936), 2253-64.

378 3. Burke, M.L. et al. (2009) Immunopathogenesis of human schistosomiasis. Parasite Immunol

379 31 (4), 163-76.

380 4. Lambertucci, J.R. et al. (2008) Imaging techniques in the evaluation of morbidity in

381 schistosomiasis mansoni. Acta Trop 108 (2-3), 209-17.

382 5. Lambertucci, J.R. (2014) Revisiting the concept of hepatosplenic schistosomiasis and its

383 challenges using traditional and new tools. Rev Soc Bras Med Trop 47 (2), 130-6.

384 6. Gryseels, B. et al. (2006) Human schistosomiasis. Lancet 368 (9541), 1106-18.

385 7. Olveda, D.U. et al. (2014) The chronic enteropathogenic disease schistosomiasis. Int J Infect

386 Dis 28, 193-203.

387 8. Andrade, Z.A. (2009) Schistosomiasis and liver fibrosis. Parasite Immunol 31 (11), 656-63.

388 9. Skelly, P.J. (2013) The use of imaging to detect schistosomes and diagnose schistosomiasis.

389 Parasite Immunol 35 (9-10), 295-301.

390 10. Olveda, D.U. et al. (2014) Utility of Diagnostic Imaging in the Diagnosis and Management

391 of Schistosomiasis. Clin Microbiol 3 (2).

392 11. Cheung, H. et al. (1996) The imaging diagnosis of hepatic schistosomiasis japonicum

393 sequelae. Clin Radiol 51 (1), 51-5.

394 12. Fung, H.S. et al. (2009) Hepatic schistosomiasis. Hong Kong Med J 15 (1), 75-6.

395 13. Goldwire, F.W. et al. (2012) A case of turtleback liver. Clin Gastroenterol Hepatol 10 (4),

396 A24.

397 14. Li, Y. et al. (2011) Severe hepatosplenic schistosomiasis: clinicopathologic study of 102
398 cases undergoing splenectomy. Hum Pathol 42 (1), 111-9.
399 15. Richter, J. et al., A Practical Guide to the Standardized Use of Ultrasonography for the
400 Assessment of Schistosomiasis-related Morbidity, Ultrasound in schistosomiasis- Second
401 International Workshop Niamey, Niger, 1996.
402 16. Huber, A. et al. (2015) State-of-the-art imaging of liver fibrosis and cirrhosis: A
403 comprehensive review of current applications and future perspectives. Eur J Radiol Open 2,
404 90-100.
405 17. Martinez, S.M. et al. (2011) Noninvasive assessment of liver fibrosis. Hepatology 53 (1),
406 325-35.
407 18. Passos, M.C. et al. (2009) Ultrasound and CT findings in hepatic and pancreatic
408 parenchyma in acute schistosomiasis. Br J Radiol 82 (979), e145-7.
409 19. Fataar, S. et al. (1985) CT of hepatic schistosomiasis mansoni. AJR Am J Roentgenol 145
410 (1), 63-6.
411 20. Manzella, A. et al. (2008) Schistosomiasis of the liver. Abdom Imaging 33 (2), 144-50.
412 21. Monzawa, S. et al. (1993) Schistosomiasis japonica of the liver: contrast-enhanced CT
413 findings in 113 patients. AJR Am J Roentgenol 161 (2), 323-7.
414 22. Nepal, P. et al. (2019) Multisystem imaging review of human schistosomiasis:
415 characteristic imaging findings. Clin Imaging 54, 163-171.
416 23. Yokoo, T. et al. (2015) Evaluation of Liver Fibrosis Using Texture Analysis on Combined-
417 Contrast-Enhanced Magnetic Resonance Images at 3.0T. Biomed Res Int 2015, 387653.
418 24. Juluru, K. et al. (2017) Diagnostic accuracy of intracellular uptake rates calculated using
419 dynamic Gd-EOB-DTPA-enhanced MRI for hepatic fibrosis stage. J Magn Reson Imaging 45 (4),
420 1177-1185.

421 25. Lambertucci, J.R. et al. (2004) Magnetic resonance imaging and ultrasound in
422 hepatosplenic schistosomiasis mansoni. Rev Soc Bras Med Trop 37 (4), 333-7.
423 26. Feier, D. et al. (2016) The diagnostic efficacy of quantitative liver MR imaging with
424 diffusion-weighted, SWI, and hepato-specific contrast-enhanced sequences in staging liver
425 fibrosis--a multiparametric approach. Eur Radiol 26 (2), 539-46.
426 27. Dragoteanu, M. et al. (2008) Staging of portal hypertension and portosystemic shunts
427 using dynamic nuclear medicine investigations. World J Gastroenterol 14 (24), 3841-8.
428 28. Kwee, S.A. et al. (2018) PET/CT with (18)F Fluorocholine as an Imaging Biomarker for
429 Chronic Liver Disease: A Preliminary Radiopathologic Correspondence Study in Patients with
430 Liver Cancer. Radiology 287 (1), 294-302.
431 29. Petroianu, A. et al. (2006) Late follow-up of patients submitted to subtotal splenectomy.
432 Int J Surg 4 (3), 172-8.
433 30. Brandt, C.T. et al. (2012) Splenosis after splenectomy and spleen tissue autoimplantation:
434 Late followup study. J Indian Assoc Pediatr Surg 17 (3), 104-6.
435 31. Ye, S. et al. (2014) F-18 FDG hypermetabolism in mass-forming focal pancreatitis and old
436 hepatic schistosomiasis with granulomatous inflammation misdiagnosed by PET/CT imaging.
437 Int J Clin Exp Pathol 7 (9), 6339-44.
438 32. de Carvalho, B.T. et al. (2016) Increased Hepatic Arterial Blood Flow Measured by Hepatic
439 Perfusion Index in Hepatosplenic Schistosomiasis: New Concepts for an Old Disease. Dig Dis
440 Sci 61 (7), 2118-26.
441 33. De Cock, K.M. (1986) Hepatosplenic schistosomiasis: a clinical review. Gut 27 (6), 734-45.
442 34. Costa Lacet, C.M. et al. (2016) Schistosomal portal hypertension: Randomized trial
443 comparing endoscopic therapy alone or preceded by esophagogastric devascularization and
444 splenectomy. Ann Hepatol 15 (5), 738-44.

445 35. Barata, C.H. et al. (1999) Abdominal ultrasound in acute schistosomiasis mansoni. Br J
446 Radiol 72 (862), 949-52.
447 36. Voieta, I. et al. (2010) Imaging techniques and histology in the evaluation of liver fibrosis
448 in hepatosplenic schistosomiasis mansoni in Brazil: a comparative study. Mem Inst Oswaldo
449 Cruz 105 (4), 414-21.
450 37. Zhang, Y.N. et al. (2019) Liver fibrosis imaging: A clinical review of ultrasound and magnetic
451 resonance elastography. J Magn Reson Imaging.
452 38. Esmat, G. et al. (2013) Fibroscan of chronic HCV patients coinfected with schistosomiasis.
453 Arab J Gastroenterol 14 (3), 109-12.
454 39. Ramzy, I. et al. (2017) Impact of old Schistosomiasis infection on the use of transient
455 elastography (Fibroscan) for staging of fibrosis in chronic HCV patients. Acta Trop 176, 283-
456 287.
457 40. Carvalho Santos, J. et al. (2018) Liver ultrasound elastography for the evaluation of
458 periportal fibrosis in schistosomiasis mansoni: A cross-sectional study. PLoS Negl Trop Dis 12
459 (11), e0006868.
460 41. Veiga, Z.S.T. et al. (2017) Transient elastography evaluation of hepatic and spleen stiffness
461 in patients with hepatosplenic schistosomiasis. Eur J Gastroenterol Hepatol 29 (6), 730-735.
462 42. Wu, S. et al. (2018) Evaluation of transient elastography in assessing liver fibrosis in
463 patients with advanced schistosomiasis japonica. Parasitol Int 67 (3), 302-308.
464 43. Ma, X. et al. (2016) Spleen Stiffness Is Superior to Liver Stiffness for Predicting Esophageal
465 Varices in Chronic Liver Disease: A Meta-Analysis. PLoS One 11 (11), e0165786.
466 44. Yoshioka, K. et al. (2008) Transient elastography: Applications and limitations. Hepatol Res
467 38 (11), 1063-8.

468 45. Ichikawa, S. et al. (2015) Comparison of the diagnostic accuracies of magnetic resonance
469 elastography and transient elastography for hepatic fibrosis. Magn Reson Imaging 33 (1), 26-
470 30.
471 46. Huwart, L. et al. (2006) Liver fibrosis: non-invasive assessment with MR elastography. NMR
472 Biomed 19 (2), 173-9.
473 47. Chou, C.T. et al. (2017) Prospective Comparison of the Diagnostic Performance of Magnetic
474 Resonance Elastography with Acoustic Radiation Force Impulse Elastography for Pre-operative
475 Staging of Hepatic Fibrosis in Patients with Hepatocellular Carcinoma. Ultrasound Med Biol 43
476 (12), 2783-2790.
477 48. Chen, J. et al. (2017) Diagnostic Performance of MR Elastography and Vibration-controlled
478 Transient Elastography in the Detection of Hepatic Fibrosis in Patients with Severe to Morbid
479 Obesity. Radiology 283 (2), 418-428.
480 49. Imajo, K. et al. (2016) Magnetic Resonance Imaging More Accurately Classifies Steatosis
481 and Fibrosis in Patients With Nonalcoholic Fatty Liver Disease Than Transient Elastography.
482 Gastroenterology 150 (3), 626-637.e7.
483 50. Park, C.C. et al. (2017) Magnetic Resonance Elastography vs Transient Elastography in
484 Detection of Fibrosis and Noninvasive Measurement of Steatosis in Patients With Biopsy-
485 Proven Nonalcoholic Fatty Liver Disease. Gastroenterology 152 (3), 598-607.e2.
486 51. Taouli, B. et al. (2007) Diffusion-weighted MRI for quantification of liver fibrosis:
487 preliminary experience. AJR Am J Roentgenol 189 (4), 799-806.
488 52. Yang, L. et al. (2018) Staging liver fibrosis with DWI: is there an added value for diffusion
489 kurtosis imaging? Eur Radiol 28 (7), 3041-3049.
490 53. Chow, A.M. et al. (2012) Liver fibrosis: an intravoxel incoherent motion (IVIM) study. J
491 Magn Reson Imaging 36 (1), 159-67.

492 54. Yu, J.S. et al. (2010) Double contrast-enhanced MRI of viral hepatitis-induced cirrhosis:
493 correlation of gross morphological signs with hepatic fibrosis. Br J Radiol 83 (987), 212-7.
494 55. Bahl, G. et al. (2012) Noninvasive classification of hepatic fibrosis based on texture
495 parameters from double contrast-enhanced magnetic resonance images. J Magn Reson
496 Imaging 36 (5), 1154-61.
497 56. Ramachandran, P. et al. (2019) Assessment of liver T1 mapping in fontan patients and its
498 correlation with magnetic resonance elastography-derived liver stiffness. Abdom Radiol (NY)
499 44 (7), 2403-2408.
500 57. Luetkens, J.A. et al. (2018) Quantification of Liver Fibrosis at T1 and T2 Mapping with
501 Extracellular Volume Fraction MRI: Preclinical Results. Radiology 288 (3), 748-754.
502 58. Wang, H.Q. et al. (2019) Assessing liver fibrosis in chronic hepatitis B using MR extracellular
503 volume measurements: Comparison with serum fibrosis indices. Magn Reson Imaging 59, 39-
504 45.
505 59. Zissen, M.H. et al. (2013) Contrast-enhanced CT quantification of the hepatic fractional
506 extracellular space: correlation with diffuse liver disease severity. AJR Am J Roentgenol 201
507 (6), 1204-10.
508 60. Polasek, M. et al. (2012) Molecular MR imaging of liver fibrosis: a feasibility study using rat
509 and mouse models. J Hepatol 57 (3), 549-55.
510 61. Hoad, C.L. et al. (2015) A study of T(1) relaxation time as a measure of liver fibrosis and
511 the influence of confounding histological factors. NMR Biomed 28 (6), 706-14.
512 62. Banerjee, R. et al. (2014) Multiparametric magnetic resonance for the non-invasive
513 diagnosis of liver disease. J Hepatol 60 (1), 69-77.
514 63. Liang, J. et al. (2018) Using IVIM-MRI and R2 Mapping to Differentiate Early Stage Liver
515 Fibrosis in a Rat Model of Radiation-Induced Liver Fibrosis. Biomed Res Int 2018, 4673814.

516 64. Zhao, F. et al. (2012) MR T1rho as an imaging biomarker for monitoring liver injury
517 progression and regression: an experimental study in rats with carbon tetrachloride
518 intoxication. Eur Radiol 22 (8), 1709-16.
519 65. Noren, B. et al. (2008) Separation of advanced from mild fibrosis in diffuse liver disease
520 using 31P magnetic resonance spectroscopy. Eur J Radiol 66 (2), 313-20.
521 66. Traussnigg, S. et al. (2017) Ultra-high-field magnetic resonance spectroscopy in non-
522 alcoholic fatty liver disease: Novel mechanistic and diagnostic insights of energy metabolism
523 in non-alcoholic steatohepatitis and advanced fibrosis. Liver Int 37 (10), 1544-1553.
524 67. Ganc, R.L. et al. (2010) Small-bowel lesions caused by portal hypertension of schistosomal
525 origin: a capsule endoscopy pilot study. Gastrointest Endosc 71 (4), 861-6.
526 68. Baekby, M. et al. (2017) Hepatosplenic schistosomiasis: playing hide-and-seek with an
527 elusive parasite. BMJ Case Rep 2017.
528 69. Koh, T.S. et al. (2008) Hepatic metastases: in vivo assessment of perfusion parameters at
529 dynamic contrast-enhanced MR imaging with dual-input two-compartment tracer kinetics
530 model. Radiology 249 (1), 307-20.
531 70. Frohlich, E. et al. (2015) Dynamic contrast-enhanced ultrasound for quantification of tissue
532 perfusion. J Ultrasound Med 34 (2), 179-96.
533 71. Leporq, B. et al. (2012) 3D-liver perfusion MRI with the MS-325 blood pool agent: a
534 noninvasive protocol to asses liver fibrosis. J Magn Reson Imaging 35 (6), 1380-7.
535 72. Ronot, M. et al. (2010) Liver fibrosis in chronic hepatitis C virus infection: differentiating
536 minimal from intermediate fibrosis with perfusion CT. Radiology 256 (1), 135-42.
537 73. Chen, B.B. et al. (2012) Dynamic contrast-enhanced magnetic resonance imaging with Gd-
538 EOB-DTPA for the evaluation of liver fibrosis in chronic hepatitis patients. Eur Radiol 22 (1),
539 171-80.

540 74. Palaniyappan, N. et al. (2016) Non-invasive assessment of portal hypertension using
541 quantitative magnetic resonance imaging. J Hepatol 65 (6), 1131-1139.
542 75. Bradley, C.R. et al. (2018) Multi-organ assessment of compensated cirrhosis patients using
543 quantitative magnetic resonance imaging. J Hepatol 69 (5), 1015-1024.
544 76. Zhang, J. et al. (2013) Gamna-Gandy bodies of the spleen detected with susceptibility
545 weighted imaging: maybe a new potential non-invasive marker of esophageal varices. PLoS
546 One 8 (1), e55626.
547 77. Li, C. et al. (2013) Magnetic resonance susceptibility-weighted imaging versus other
548 imaging modalities in detecting splenic siderotic lesions. PLoS One 8 (9), e73626.
549 78. Bezerra, A.S. et al. (2007) Chronic hepatosplenic schistosomiasis mansoni: magnetic
550 resonance imaging and magnetic resonance angiography findings. Acta Radiol 48 (2), 125-34.
551 79. Bezerra, A.S. et al. (2008) Differentiating cirrhosis and chronic hepatosplenic
552 schistosomiasis using MRI. AJR Am J Roentgenol 190 (3), W201-7.
553 80. Balassy, C. et al. (2014) Susceptibility-weighted MR imaging in the grading of liver fibrosis:
554 a feasibility study. Radiology 270 (1), 149-58.
555 81. Andrade, Z.A. et al. (1997) An experimental approach to the pathogenesis of "pipestem"
556 fibrosis (Symmers' fibrosis of the liver). Mem Inst Oswaldo Cruz 92 (5), 699-706.
557 82. Sarin, S.K. et al. (1991) Hyperdynamic circulation in a chronic murine schistosomiasis
558 model of portal hypertension. Hepatology 13 (3), 581-4.
559 83. Stuker, F. et al. (2011) Fluorescence molecular tomography: principles and potential for
560 pharmaceutical research. Pharmaceutics 3 (2), 229-74.
561 84. Krautz-Peterson, G. et al. (2009) Imaging schistosomes in vivo. Faseb j 23 (8), 2673-80.
562 85. Salem, N. et al. (2010) In vivo imaging of schistosomes to assess disease burden using
563 positron emission tomography (PET). PLoS Negl Trop Dis 4 (9).

564 86. Holtfreter, M.C. et al. (2011) Confocal laser scanning microscopy for detection of
565 Schistosoma mansoni eggs in the gut of mice. PLoS One 6 (4), e18799.
566 87. Fritzsche, C. et al. (2012) Confocal laser scanning microscopy, a new in vivo diagnostic tool
567 for schistosomiasis. PLoS One 7 (4), e34869.
568 88. Suff, N. and Waddington, S.N. (2017) The power of bioluminescence imaging in
569 understanding host-pathogen interactions. Methods 127, 69-78.
570 89. Mezzanotte, L. et al. (2017) In Vivo Molecular Bioluminescence Imaging: New Tools and
571 Applications. Trends Biotechnol 35 (7), 640-652.
572 90. Davies, S.J. et al. (2005) In vivo imaging of tissue eosinophilia and eosinopoietic responses
573 to schistosome worms and eggs. Int J Parasitol 35 (8), 851-9.
574 91. Harvie, M.C.G. et al. (2019) Live imaging of collagen deposition during experimental
575 hepatic schistosomiasis and recovery: a view on a dynamic process. Lab Invest 99 (2), 231-243.
576 92. Maezawa, K. et al. (2018) Real-time observation of pathophysiological processes during
577 murine experimental Schistosoma japonicum infection using high-resolution ultrasound
578 imaging. Trop Med Health 46, 1.
579 93. Cheng, P.C. et al. (2013) Evaluating the potential of a new isotope-labelled glyco-ligand for
580 estimating the remnant liver function of schistosoma-infected mice. Parasite Immunol 35 (3-
581 4), 129-139.
582 94. Kosaka, M. et al. (2000) In vivo NMR micro-imaging of kidney and liver of mouse at 9.4 T.
583 Jpn J Physiol 50 (4), 463-7.
584 95. Masi, B. et al. (2015) In Vivo MRI Assessment of Hepatic and Splenic Disease in a Murine
585 Model of Schistosomiasis [corrected]. PLoS Negl Trop Dis 9 (9), e0004036.
586 96. Schuppan, D. et al. (2018) Liver fibrosis: Direct antifibrotic agents and targeted therapies.
587 Matrix Biol 68-69, 435-451.

588 97. Suk, K.T. (2014) Hepatic venous pressure gradient: clinical use in chronic liver disease. Clin
589 Mol Hepatol 20 (1), 6-14.
590 98. Bonnard, P. et al. (2015) Comparison of liver biopsy and noninvasive techniques for liver
591 fibrosis assessment in patients infected with HCV-genotype 4 in Egypt. J Viral Hepat 22 (3),
592 245-53.
593 99. Kardorff, R. et al. (2003) Validation of ultrasonography for hepatic schistosomiasis using a
594 porcine Schistosoma japonicum model. Acta Trop 85 (3), 315-23.
595 100. Standley, C.J. et al. (2013) Intestinal schistosomiasis in chimpanzees on Ngamba Island,
596 Uganda: observations on liver fibrosis, schistosome genetic diversity and praziquantel
597 treatment. Parasitology 140 (3), 285-95.
598 101. Liang, X.L. and Yuan, J.Y. (2013) Effect of Chinese herbal compound on liver fibrosis in
599 rabbits with schistosomiasis by B-ultrasound. Asian Pac J Trop Med 6 (8), 658-62.
600
601

HIGHLIGHTS

- Liver fibrosis and portal hypertension in HSS may lead to variceal bleeding.
- Fibrogenesis in HSS differs from fibrogenesis of other etiology and requires specific and sensitive markers covering fibrosis heterogeneity. Currently no imaging markers are specific for HSS.
- USG is the leading imaging modality for HSS diagnosis, but other diagnostic imaging techniques can quantify liver fibrosis.
- Quantitative markers of HSS (collagen, iron and calcium deposition, microvascular density and flow) became accessible by medical imaging modalities.
- Semiquantitative and quantitative imaging markers for the assessment of vascular and hemodynamic alterations constitute valuable markers for staging, prognosis and treatment response.
- Preclinical imaging studies of HSS contribute to the development of clinically transferable markers sensitive to granulomatous inflammation and mild fibrosis.

GLOSSARY

Arterial spin labelling (ASL): Quantitative microvascular perfusion MRI technique relying on magnetically labeled arterial blood water molecules as endogenous tracer.

Bioluminescence imaging (BLI): whole-animal imaging method requiring the introduction of a bioluminescent reporter gene (*e.g.* firefly luciferase gene) fused to a gene of interest. When the luciferase substrate is injected to the animals, its oxidation results into detectable light emission.

626 **Contrast agents (CA):** mostly intravenously injected small molecules, which have the capacity
627 to enhance tissue contrast by modifying signal intensity upon accumulation. MRI CAs:
628 paramagnetic agents modifying the relaxation of neighbouring water protons. CT CAs contain
629 atoms with high atomic number increasing local photoelectric absorption. USG CAs: gas-
630 containing microbubbles.

631 **Deoxy-2-(^{18}F)fluoro-D-glucose:** a non-metabolizable glucose derivative used as radiotracer to
632 assess glucose uptake in activated cells with PET imaging.

633 **Diffusion MRI:** unique imaging modality capable of probing tissue microstructure by
634 measuring the water diffusivity which is hindered by biological barriers (*e.g.* cell membranes).

635 **Dynamic contrast enhancement (DCE):** following intravenous injection of a CA bolus,
636 different phases of signal changes occur that are analysed using a pharmacokinetic model. The
637 main phases are the arterial, portal venous and parenchymal phase in chronological order
638 providing information about microvascular hemodynamics and CA distribution volume.

639 **Elastography:** method allowing the quantification of tissue stiffness (resistance to
640 deformation) following the propagation of a mechanical strain or shear wave.

641 **Fluorescence molecular tomography (FMT):** whole-animal imaging method requiring the
642 injection of a fluorescent dye and irradiation with an excitation laser to generate light emission.

643 **Intravoxel incoherent motion (IVIM):** a mathematical model distinguishing two
644 contributions to the total tissue diffusivity in diffusion MRI: the microvascular
645 (pseudodiffusivity D* weighted by the perfusion fraction f_{IVIM}) and the extravascular diffusivity
646 D.

647 **Magnetic resonance spectroscopy (MRS):** a spectroscopic modality allowing to identify and
648 to quantify biochemical molecules by analysing the resonance frequency of electromagnetic
649 waves emitted by atomic nuclei with magnetic properties such as ^{1}H and ^{31}P.

650 **Quantitative susceptibility mapping (QSM):** a parametric map of the tissue magnetic
651 susceptibility generated by the presence of para- and diamagnetic compounds and obtained by
652 deconvolution of the magnetic field distributions in T_2* weighted MRI
653 **Relaxometry:** measurement of magnetic relaxation time constants describing the return to
654 equilibrium of excited nuclei (longitudinal T_1, (true) transverse T_2, (observed) transverse T_2*,
655 mixed $T_1\rho$. Magnetic relaxation is affected by molecule mobility and environment.
656 **Voxel:** volume element equivalent to a three-dimensional pixel.
657
658 **Box 1. Liver fibrosis and portal hypertension in hepatosplenic schistosomiasis**
659 Liver fibrogenesis is a wound-healing process activated by an inflammatory trigger and
660 perpetuated by chronic inflammation. In schistosomiasis, a moderate Th1 response occurs,
661 followed by a shift to a strong Th2 response elicited by egg antigens. The eggs become
662 surrounded by immune cells. IL13 stimulates hepatic stellate cells (HSCs), the major ECM-
663 producing cells, serving as vitamin A reservoirs and modulating vascular resistance and
664 sinusoidal blood flow. Sinusoids are fenestrated vessels receiving blood from terminal hepatic
665 arterioles and portal venules and delivering oxygen and nutrients to hepatocytes. Quiescent
666 HSCs located in the space of Disse separating sinusoidal endothelial cells from adjacent
667 hepatocytes and containing connective tissue trans-differentiate into phenotype-like
668 myofibroblasts with increased contractile properties. They lose their vitamin A-containing lipid
669 droplets and secrete fibrous collagens, fibronectin and proteoglycans, together with matrix
670 metalloproteinases (MMPs) degrading ECM and tissue inhibitors of metalloproteinases
671 (TIMPs) regulating their proteolytic activity. The imbalance between ECM synthesis and
672 degradation progressively leads to replacement of liver tissue by a fibrous scar (fibrosis),
673 resulting in increased liver stiffness and distorted vascular architecture. Fibrosis is potentially
674 reversible, even in advanced stages. The therapeutic strategies explored to reverse fibrosis

675 target either the inhibition of fibrogenetic mechanisms or fibrolysis but clinical validation is
676 needed [96]. Grading scales for fibrosis based on histology (*e.g.* METAVIR score) or serum
677 markers exist but are not specific for schistosomiasis. Cirrhosis is the end-stage of liver fibrosis
678 and is characterized by regenerative nodule formation, distorted hepatic vasculature, portal
679 hypertension and liver dysfunction.
680 Portal hypertension is the main complication of liver fibrosis and is defined by an elevation of
681 the hepatic venous pressure gradient (HVPG) above 5 mmHg. A value of 10 mmHg is
682 indicative of clinically patent PH with a high risk of developing varices [97]. In HSS, periportal
683 fibrosis and granulomatous thrombophlebitis lead to progressive presinusoidal blood flow
684 obstruction (terminal portal venules level) and increased hepatic resistance causing PH. PH is
685 complicated by congestive splenomegaly, formation of Gamna-Gandy bodies containing iron
686 and calcium inclusions, varices, destruction of the main portal vein branches despite the
687 development of portosystemic collateral blood flow that may partly decompress the portal
688 system and at end-stage by life-threatening variceal bleeding. Gastrointestinal bleeding is often
689 the first clinical sign of PH. The management of PH may be pharmacological with the
690 prophylactic administration of β-blocker propanolol, or surgical with portacaval shunt, varice
691 devascularization and splenectomy, distal splenorenal shunt, or with endoscopic sclerotherapy
692 or ligation.
693

694 **OUTSTANDING QUESTIONS**
695
696
697 • Some patients progress to severe HSS, while patients with strong immunologic
698 modulation capacity develop less severe (intestinal or hepatointestinal) variants of
699 the chronic disease. Can imaging examinations of hepatic manifestations of acute
700 schistosomiasis have prognostic potential?

701 • How reliable is the non-invasive imaging assessment of fibrosis at early stages of
702 the disease?
703 • Can we disentangle confounding factors to quantitative fibrosis markers (*e.g.*
704 comorbidities, inflammation, iron overload)?
705 • Is a detailed classification equivalent to the Niamey USG classification (made for *S.*
706 *mansoni* infection) needed for *S. japonicum* HSS?
707 • Should the Niamey USG classification be refined to include novel measurable
708 markers by more advanced USG equipment *(e.g.* hemodynamics, vascular
709 morphology, microbubble contrast enhancement, DCE)?
710 • Will the establishment of new guidelines and standardized protocols for imaging
711 modalities other than USG be of diagnostic and prognostic utility?
712 • What is the (multiparametric) imaging protocol best suited for reliable diagnosis and
713 staging of HSS patients?
714 • Will the ASL technique and the newly-developed DCE-USG technique allow the
715 assessment of hemodynamic alterations in HSS?
716

Table 1. General features of clinical abdominal imaging modalities

	USG	CT	MRI	Scintigraphy+ SPECT	PET	Endoscopy/Laparoscopy
Portability	Yes	No	No	No	No	Portable equipment used in surgical setting
Cost of equipment	≈ 30k $	≈ 1M $	>1M $	γ-camera ≈ 0.5M $	PET+CT≈ 2M $	< 25k $
Invasiveness	No*	No*	No*	Yes	Yes	Yes, anesthesia required
Scanning/exam time	Real-time imaging / 5 - 20 min	30 s / 10 min**	5 / 30 min**	30 min / 4 h	20 min/ radionuclide injected 1 h before	Real-time imaging/ 1-2 h for preparation
Basic principle / type of radiation-tissue interaction	Propagation of pulses of ultra-high frequency (1 to 20 MHz) acoustic waves. US reflection at tissue interfaces with differing impedances and their diffusion in tissue parenchyma provide	External irradiating tomographic method using X-ray photon transmission to obtain image contrast based on the attenuation	Absorption and reemission of radiofrequency electromagnetic waves by nuclear magnetic resonance of tissue hydrogen when placed in a strong external magnetic field. Image contrast is obtained by magnetic relaxation, local susceptibility differences and	Internal irradiating method involving the injection of labelled biomolecules (radiotracers) and based on the detection of the emitted γ-ray photons after distribution.	Internal irradiating method involving the injection of labelled biomolecules (radiotracers) and based on the detection of γ-ray photons emitted in the annihilation	Introduction of flexible or rigid tubes into internal hollow organs or cavities conducting visible light *via* optic fibres for endoluminal images of epithelium.

	morphological information in brightness (B) mode. The Doppler frequency shift of the wave reflected by blood cells provides hemodynamic information.	coefficients of the tissues.	water motion due to flow, diffusion or tissue deformation.		process between positrons from the radiotracer with electrons from tissue.	
Principal imaging applications	Anatomical imaging (tissue interfaces, echogenicity, texture) Functional imaging Image-guided intervention	Anatomical imaging Perfusion imaging Image-guided intervention	Multiparametric anatomical imaging Functional/physiological imaging Metabolic imaging Image-guided intervention	Functional / physiological imaging Metabolic imaging Image-guided intervention	Functional / physiological imaging Metabolic imaging Image-guided intervention	Anatomical imaging of tissue surfaces Image-guided intervention
Use of contrast agents (CA) or radiotracers (RT)	CEUS with injection of microbubbles as reticuloendothelial or blood pool CA for the characterization of focal liver lesions, vascular	CA: mainly non-specific iodine - containing agents	CA: non-specific extracellular gadolinium chelates for perfusion imaging and parenchymal contrast enhancement, hepatocyte-specific gadolinium and	RT: ^{99m}Tc labelled molecules most widely used	RT: ^{18}F, ^{15}O, ^{13}N, ^{11}C labelled molecules (ie: ^{18}F 2-Deoxy Glucose)	Topically or systemically administered targeted fluorescent CA for molecular endoscop

	imaging and therapy monitoring		manganese chelates taken up by functioning hepatocytes only, superparamagnetic iron oxide (SPIO) particles targeting Kupffer cells			
Spatial resolution (range)	0.3 to 1.5 mm depending on US frequency	0.3 to 1 mm depending on X-ray tube dimensions and detector size	0.5 to 3 mm depending on acquisition time, magnetic field strength and gradient coils	5 to 12 mm depending on collimator and detector system	4 to 10 mm depending on detector size	< 0.1 mm depending on camera matrix
Penetration depth	1 to 30 cm depending on US frequency, US probe can be inserted into gastrointestinal tract	Limitless	Limitless	Limitless	Limitless	Superficial
Soft tissue contrast	Good	Medium	Excellent	NA	NA	Visual contrast
Vascular imaging -Anatomy of vessels (AV)	AV: 2D, angiography, venography. HD: blood flow, blood volume, velocity,	AV: 2D and 3D angiography, venography. HD: blood flow, blood volume, velocity,	AV: 2D and 3D, angiography, venography. HD: blood flow, blood volume, velocity, perfusion. CA injection not necessary	HD : blood flow	HD: blood flow	AV: limited to superficial mucosal vessels, improved with narrow band imaging (higher relative intensity of blue light)

-Hemodynamics (HD)	using Color encoded Doppler, Power Doppler (B-flow) or CEUS	arterial, venous and perfusion phases, using CA injection				
Organ volumetry	Multiplanar 2D imaging, volumetric analysis with 3D option	Axial 2D and 3D imaging	Multiplanar 2D and 3D imaging	2D and 3D imaging	3D but requires CT or MRI for anatomical location	Size estimation from organ surface view (images, videos)
Fibrosis assessment	Organ surface morphology, parenchymal echogenicity, elastometry or elastography	Morphology, texture analysis	Morphology, texture analysis, hepatocyte specificCA, **relaxometry**, diffusion MRI, elastography, ^{31}P-MRS	^{99m}Tc-labelled sulphur colloid particles	^{18}F fluorocholine	Organ surface morphology
Detection of splenic siderotic nodules	Hyperechogenic parenchymal foci, acoustic shadowing if calcified	Attenuation dependent on calcification, hypodense on contrast enhanced CT	Hypointense lesion on T_1w MRI, T_2w MRI, SWI, even after CA administration	No	No	No
Theranostic applications	Use of high intensity focussed ultrasounds (HiFu) for abdominal cancer treatment	(Preclinical research)	(Preclinical research)	Yttrium for liver cancers	(Preclinical and clinical research)	Theranostic capsule endoscopy (research) Fluorescence imaging endoscopy with nanoparticles (research)

Limitations	Operator dependent, qualitative signal yielding only relative echogenicity, few images are usually saved, limited field of view, decreasing image quality and spatial resolution with depth, acoustic shadowing by gas, gallstones and bone	Allergic risk to Iodine-based CA observed in up to 0.7%, repeated exposure to ionising radiations not recommended,	Long scan times, sensitivity to motion, absolute contraindications exist, precautions regarding radiofrequency energy absorption are required, possible interference with vital medical electronic devices, CA with rare adverse reactions (<0.01%) but contraindicated in patients with renal insufficiency	Main applications in oncology, Co-registration with CT or MRI often necessary for better anatomical localization of radiotracers, cumulative exposure to internal (radiotracers) and external (CT) ionizing radiation	Few scanners available, main application in oncology Co-registration with CT or MRI often necessary for better anatomical localization, cumulative exposure to internal (radiotracers) and external (CT) ionizing radiation	Qualitative images limited to surface of the organ or cavity Sedation or anesthesia required, surgical team needed, infectious risk

* non-invasive technique in the absence of contrast agent injection; ** depending on protocols; CEUS = contrast enhanced ultrasound; NA= not applicable; T_1w = T_1-weighted MRI; T_2w = T_2-weighted MRI, US = ultrasound.

Table 2. Assessment of human HSS morbidity with abdominal imaging modalities

Imaging findings in hepatosplenic schistosomiasis	Disease stage	USG	CT	MRI	Scintigraphy / SPECT	PET	Endoscopy
Schistosome visualisation	Acute stage Chronic stage	In combination with endoscopy	No	No	No	No	No
Granulomatous inflammation	Chronic stage	Yes Echogenic structure	With and without CA	Anatomical MRI	Yes	^{18}FDG	Yes (laparoscopy)
Liver fibrosis (Symmers pipestem fibrosis)	Chronic stage	Yes, standard patterns, measurement of portal vein, gall bladder and fibrosis of second order branches	Measurement of portal vein, gall bladder and fibrosis of portal vein branches	Measurement of portal vein, gall bladder and fibrosis of portal vein branches	No	No	In advanced stage fibrosis visible at the liver surface by laparoscopy
Portal hypertension	Chronic stage	Portal vein diameter, blood flow and velocity Doppler USG	Portal phase after CA injection, detection of vessel dilation	Anatomical MRI	hepatic angioscintigraphy with 99mTc-labelled sulphur colloid particles	No	Yes, qualitative (laparoscopy)

Hepatomegaly	Acute stage Chronic stage	Qualitative evaluation and organ axis measurements, no volumetric analysis without 3D option	Yes, volumetric analysis	Yes, volumetric analysis	Qualitative	No	Yes, qualitative (laparoscopy)
Splenomegaly	Acute stage Chronic stage (severe HSS)	Qualitative evaluation and organ main axis measurement, no volumetric analysis without 3D option	Yes, volumetric analysis	Yes, volumetric analysis	Yes, volumetric analysis	No	Yes, qualitative (laparoscopy)
Gall bladder abnormalities	Chronic stage	Yes, wall thickness measurement	Yes, wall thickening and inflammation visible	Yes, wall thickening and inflammation visible	No	No	Yes, if reaching the gall bladder surface
Esophageal varices	Chronic stage (severe HSS)	Yes with special probe	Yes, venography	Yes, venography	No	No	Yes, gold standard
Visceral collaterals	Chronic stage (severe HSS)	USG angiography, Doppler USG	Angiography with CA	Angiography	No	No	Yes, qualitative (laparoscopy)
Splenic siderotic nodules	Chronic stage	Hyperechogenic parenchymal foci, acoustic shadowing if calcified	Attenuation dependent on calcification, hypodense on contrast enhanced CT	Hypointense lesion on T_1-w MRI, T_2-w MRI, SWI, even after CA administration	No	No	No
Ascites	Chronic stage (severe HSS)	Anechoic fluid	Hypodense with respect to liver parenchyma	Anatomical MRI	No	No	Yes, qualitative (laparoscopy)

CT= computed tomography; MRI= magnetic resonance imaging; PET= positron emission tomography; SPECT= Single-photon emission computed tomography; T_1w= T_1-weighted MRI; T_2w= T_2-weighted MRI; USG = Ultrasonography.

Table 3. Assessment of liver fibrosis in HSS with elastography[1]

References	Comorbidities	Parasite strain	Population characteristics	Elastographic method	Additional Imaging modalitie(s)	Main findings	Limitations
[40]	None	*S. mansoni*	-358 Brazilian patients, among them 86 with mild periportal fibrosis (Niamey C pattern) and 272 with advanced periportal fibrosis (Niamey D, E, F patterns)	Point shear wave elastography, ARFI	USG with a 6C1 MHz transducer for USG and elastography	Differentiation between mild and advanced periportal fibrosis	USG and elastography performed by the same sonographer
[42]	None	*S. japonicum*	-106 Chinese patients with advanced schistosomiasis and no current infection, among them 80 patients without comorbidities (blood tests with biochemical assessment of liver function and fibrosis, percutaneous liver biopsy) -Conclusive results obtained on 73 patients (METAVIR score: 3 F0, 11 F1, 22 F2, 24 F3, 13 F4)	Transient elastography, FibroScan	USG classification into 5 grades, Doppler USG, histology	-No correlation between LSM and USG grading but good correlation with histology -LSM superior to blood serum analysis for detection of fibrosis and cirrhosis and predictive of fibrosis in patients	No USG-based classification of liver fibrosis (Niamey patterns)

						with advanced schistosomiasis japonica	
[41]	None	*S. mansoni*	-77 Brazilian patients: 30 with hepatosplenic schistosomiasis (24% Niamey B pattern, 28% Niamey C pattern, 48% Niamey D pattern), 30 patients with HCV cirrhosis and 17 controls	Transient elastography, FibroScan	USG with Doppler-fluxometry, ultrasound color Doppler	- Increased LSM values in patients with schistosomiasis compared to controls -Increased spleen stiffness, comparable to that of cirrhotics _increased spleen stiffness correlated with portal hypertension	- Absence of severe fibrosis (*e.g.* patterns E or F) - differentiation of schistosomiasis patients from cirrhotic patients by LSM could be biased
[39]	HCV	Unknown, *S. mansoni* most likely	-352 Egyptian patients with chronic HCV hepatitis (no decompensated cirrhosis, no HCC): 122 controls, 122 with positive antischistosomal antibodies and without periportal tract thickening,	Transient elastography, FibroScan	USG	-No difference in liver stiffness among groups -Best correlation between METAVIR score and LSM in	No USG-based classification of liver fibrosis (Niamey patterns)

			108 with positive antischistosomal antibodies and periportal tract thickening -Liver biopsies and METAVIR scores available			patients with HCV only -Only higher antischistosomal antibody titres reduce the correlation between METAVIR score and LSM	
[98]	HCV	Unknown, *S. mansoni* most likely	-312 Egyptian patients with HCV genotype 4, among them 36 with positive schistosomiasis serology, and 4 with hepatic schistosomiasis lesions detected on liver biopsy	Transient elastography, FibroScan	No	No influence of positive schistosomiasis serology on elastography results	Very small number of patients with schistosomiasis lesions
[38]	HCV	Unknown, *S. mansoni* most likely	-231 Egyptian patients with chronic HCV, among them 67 patients presenting positive schistosomal serology -Liver biopsies and METAVIR scores: 31 F0-F1, 13 F2, 14 F3 and 9 F4	Transient elastography, FibroScan	No	Positive schistosomal serology impairs correlation between FibroScan results and METAVIR score (more obvious in F2 and F3 stages)	No USG-based classification of liver fibrosis (Niamey patterns)

*Transient elastography and Point shear wave elastography are strictly speaking no imaging modalities since LSM is performed in a point at a particular depth. Transient elastography uses a one-dimensional USG signal for guidance, while Point shear wave elastography relies on 2D USG for determining the measurement point. ARFI = acoustic radiation force imaging; HCV = Hepatitis C virus; HCC = hepatocellular carcinoma; LSM= Liver Stiffness Measurement; USG = Ultrasonography.

Table 4. Preclinical imaging studies of schistosomiasis

References	Imaging modalities and methods	Animal model and groups	Parasite, number of cercariae and mode of infection	Observation period	Assessment of pathogenic features	Main findings	Potential applications
[91]	BLI, endogenous expression of luciferase under a collagen promotor	Male and female B6.Coll 1A-luc+ mice (C57BL6/J background) SjC mice (n=12), SjP mice (n=14) SjC mice treated with PZQ (n=10), SjP mice treated with PZQ (n=10) Control group (n=5)	*S. japonicum (SjC,* Chinese origin, 35 cercariae) and *SjP* (Philippines origin, 14 cercariae)	From week 4 to 10 post infection for SjC mice, and from week 4 to 11 post infection for SjP	-Collagen deposition with BLI and comparison with histology	-Dynamic assessment of collagen deposition before and after PZQ treatment	-Assessment of antifibrotic drug effects in infected mice
[92]	USG, classic (18–4 MHz human probe) and high-resolution (50 MHz probe, resolution 30 µm)	5-week old infected BALB/C female mice (n=22) and controls (number unknown)	*S. japonicum* (Yamanashi strain), 25 cercariae (n=12) and 10 cercariae (n=10), percutaneous route	Up to 13 weeks (n=12) and one year (n=10) post infection	-Morphometry of spleen and liver, signs of PH, intestinal wall thickening,	-Visualisation of live worms in portal vein -Real-time evaluation of schistosomiasis impact on digestive organs	-Studies of new anti-parasitic drugs on worms, longitudinal preclinical studies (therapy, molecular

					echogenic patterns of liver fibrosis		mechanisms of disease, transfer to the clinical setting)
[95]	MRI @11.75T, 2D anatomical MRI with and without Gd-DOTA injection Relaxometric studies (T_2 mapping, T_2* mapping) comparison with histology	6-week old CBA/J female mice, infested mice (n=12) and controls (n=12)	*S. mansoni,* 30 *cercariae,* percutaneous route	2, 6 and 10 weeks post infection	-Liver and spleen volumetry, and PH assessment with anatomical MRI -Fibrosis assessment with relaxometry and histology	-Detection of indirect signs of PH -Quantification of splenomegaly and hepatomegaly -Identification of T_2 relaxation time as a marker for liver fibrosis	-Longitudinal studies of antifibrotic drug effects, mechanistic studies on genes or immune molecules involved in fibrogenesis -Transfer to the clinical setting
[93]	MicroSPECT/CT with injection of 188Re-OCTAM	6 to 8-week old BALB/C male mice, divided in 3 groups of infected mice and one control group (n=7-10 per group)	*S. mansoni* (Puerto Rican strain), 100 cercariae, percutaneous route	Imaging at 1, 4, 24 and 48h post injection of 188Re-OCTAM, 9, 12 and 18 weeks post infection	-Liver inflammation, necrosis and fibrosis	-Identification of various levels of remnant liver function in different stages of the disease	-Longitudinal studies of antifibrotic drug effects, mechanistic studies on genes or immune molecules involved in fibrogenesis

[85]	micoPET using ^{18}FDG + FMT with near-infrared imaging agent MRI @7T for T_2-weighted images with contrast agent, comparison with histology	6-week old female nude mice (nu/nu) Infected mice (n=35) and controls (n=4), 6 mice treated with PZQ	*S. mansoni*, number of cercariae unknown, percutaneous route	5-6 weeks post infection	-Localization and quantification of schistosome worms	-^{18}FDG fixed by *S mansoni* worms -In vivo quantification of the worm burden with ^{18}FDG PET	-Studies of new anti-parasitic drug effects on worms -*In vivo* parasite detection in humans
[84]	FMT with near-infrared imaging agent	6 to 8-week old female BALB/c mice (exact number unknown)	*S. mansoni* (Puerto Rican strain), 100 or 50 cercariae per mouse, *S. hematobium,* 25 cercariae per mouse and *S. Japonicum,* 25 cercariae per mouse, percutaneous route	5 weeks *(S. Mansoni)*, 8 weeks *(S. Hematobium*) and 6 weeks *(S. Japonicum)* post infection	-Localization and quantification of schistosome worms	-New method to detect, quantify and localize worms	-Studies of new anti-parasitic drug effects on worms
[90]	BLI, genetically encoded luciferase (luc) reporter driven by an eosinophil peroxidase (EPX) promoter, intraperitoneal injection of luciferase substrate luciferin	EPX334-luc or EPX339-luc mice and EPX-luc hemizygous mice as controls (age and exact number unknown)	*S. mansoni*, 50 cercariae, subcutaneous route	Over 12-week period post infection	-Eosinophilia and eosinopoiesis	-Detection and quantification of eosinophilia and eosinopoiesis in schistosomiasis -First *in vivo* description of	-Study of molecules modulating eosinophilia and eosinopoiesis in schistosomiasis

						eosinopoietic response to schistosomes	
[94]	MRI @9.4T, anatomical T_1, T_2, T_2*-weighted MRI, no contrast agent	10 to 20-week old BALB/C infected mice and controls (exact number unknown)	*S. mansoni*, 150 cercariae, subcutaneous route	Followed for 13 weeks post infection	-Assessment of liver disease and involvement of intrahepatic bile ducts	-Patchy pattern in the liver related to fibrosis after 6 weeks of infection	-Anatomical MRI for the assessment of liver disease in preclinical studies
[99]	USG with a system for human imaging (multifrequent convex array probe of 3.5/4.3/5.0 MHz)	12-week old female and castrated male pigs (Danish landrace x Duroc and or Hampshire crossbreeds) Infected pigs (n=9) and uninfected controls (n=10)	*S. japonicum,* 1000 cercariae of Chinese origin. Route of injection not documented.	Imaged 12 weeks after infection	-Assessment of HSS disease, comparison of USG findings with histology	-Enlarged liver Diffuse parenchymal alterations -Echogenic portal thickening -Enlarged portal vein diameter	-Validation of the swine model of schistosomiasis as a good model of human HSS
[100]	Portable USG	8 semi-captive chimpanzees (Uganda), infected by *S. mansoni,* under PZQ treatment but still excreting schistosome eggs	*S. mansoni* (naturally infected animals)	USG included in the annual health assessment of infected animals	-Assessment of intestinal disease and progression toward HSS. -Parasitological assessment (urine and stools)	-Detection of a spectrum of fibrosis stages including mild disease, pipestem fibrosis and occluding fibrosis.	-Detection of fibrosis patterns identical to those described in humans (Niamey protocol)

					-DNA schistosome barcoding	-DNA schistosome diversity	Probable zoonosis (chimpanzees, humans, snails)
[101]	USG (B mode)	24 male New-Zealand rabbits infected with *S. japonicum* used for the assessment of the anti-fibrotic effects of Chinese traditional medicine -6 animals received PZQ -6 animals received *Radix astragali and Salvia miltiorrhiza* -6 animals received *Radix astragali and Angelica sinensis* -6 animals received *Radix astragali, Salvia miltiorrhiza, Angelica sinensis* and PZQ	*S. japonicum,* 100 cercariae, percutaneous route	-Treatment started 18 weeks post infection, -Weekly USG from week 13 until week 28	-Assessment of HSS in liver (liver diameter, PV inner diameter, echogenic septa forming mosaics, echogenic spots) -Assessment of serum markers of fibrosis and liver function -Comparison of the effects of traditional Chinese medicines to PZQ on liver fibrosis	Validation of the rabbit model of HSS obtained with *S. japonica* Beneficial effects of traditional Chinese medicines on liver fibrosis	Assessment of antifibrotic drug effects in a good model of the human disease resulting from *S. japonicum* infection

Abbreviations: BLI = bioluminescent imaging; CT= computed tomography; EPX= eosinophil peroxidase promoter; FMT= Fluorescence molecular tomography; LSM= Liver Stiffness Measurement; luc= luciferase; MRI= magnetic resonance imaging; PET= positron emission tomography; PH = portal hypertension; PV= portal vein; PZQ= praziquantel; SPECT= Single-photon emission computed tomography; USG = Ultrasonography.

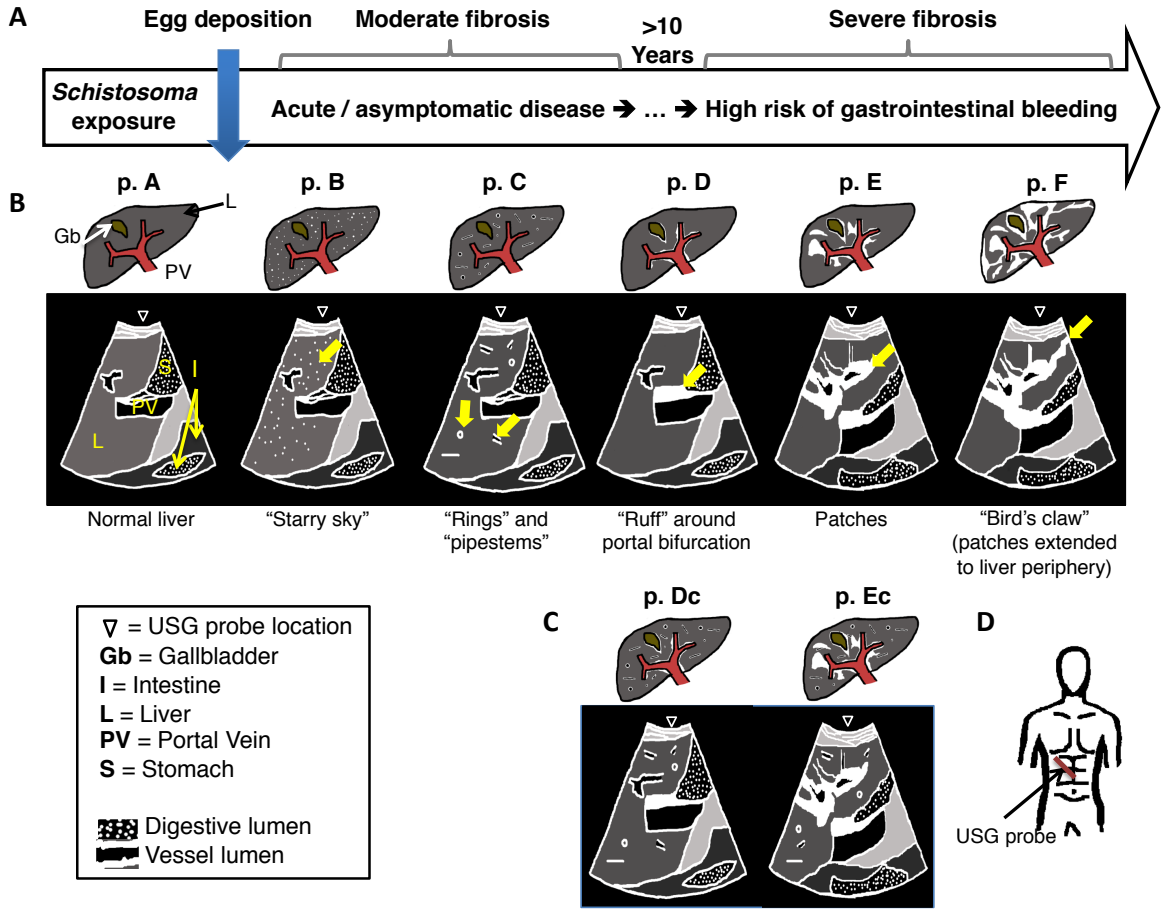

Figure 1, Key Figure. Schematic representations of typical USG images in HSS and corresponding patterns based on Niamey classification. A. Temporal progression of HSS. **B.** Illustration of the different stages of HSS with Niamey classifications patterns (top row) and corresponding schematic representations of USG images (bottom row). The right oblique ultrasound probe orientation allows visualisation of the hepatic hilar area with the portal vein (PV) and surrounding vessels. This view allows detection of periportal fibrosis (pattern D to Ec) and measurement of PV diameter as well as evaluation of hypertension (dashed line in D, E and F patterns). Pattern B (p. B) also named "Starry sky" corresponds to echogenic spots in liver parenchyma caused by inflammation and fibrosis around granuloma. Pattern C (p. C) shows echogenic signals around portal branches and represents a moderate stage of fibrosis. Acute or/and asymptomatic phases are assigned to B and C patterns. Large fibrosis areas in

parenchyma, described as “patches”, are associated with E pattern. Fibrosis extension to the liver periphery from patches was described as “Bird’s claw” and assigned to F pattern. **C.** Dc and EC are examples of combined patterns. **D.** Right echographic oblique view presented in **B**.